RSC Advances

ROYAL SOCIETY OF CHEMISTRY

www.rsc.org/advances

Table of contents

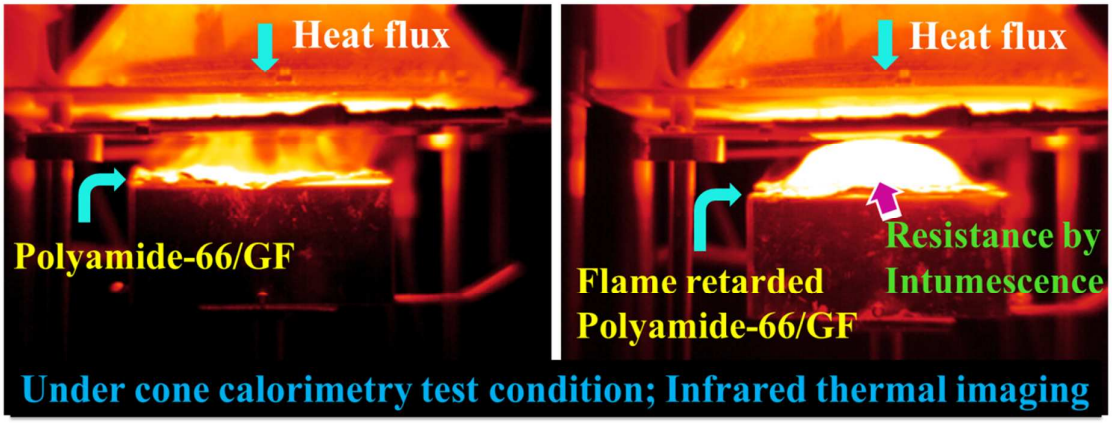

Text:

Multimodal action and synergism of Melamine poly(aluminum phosphate) in the flame retardancy of polyamide 66

RSC Advances

RSCPublishing

ARTICLE

Mapping the multimodal action of Melamine-poly(aluminium phosphate) in the flame retardancy of polyamide 66

Cite this: DOI: 10.1039/x0xx00000x

Received ooth January 2012,
Accepted ooth January 2012

DOI: 10.1039/x0xx00000x

www.rsc.org/

Anil D. Naik,[a] Gaëlle Fontaine,[a] Fabienne Samyn,[a] Xavier Delva,[b] Jérémie Louisy,[b] Séverine Bellayer,[a] Yann Bourgeois,[b] and Serge Bourbigot*[a]

A higher analogue in the melamine polyphosphate family, Melamine-poly(aluminium phosphate) (Safire®200), that has shown flame retardancy along with aluminium phosphinate in glass-fibre reinforced polyamide 66 was investigated to elucidate their mode of action. The mechanistic investigation is based on examining the chemical species formed in the condensed and gas phase under different fire scenario. Samples at different stages of degradation were collected based on heat release rate (HRR) curve of cone calorimeter and further analysed. Additionally, formulations and flame retardants were also pyrolysed at characteristic temperatures in tubular furnace based on their thermogravimetric analysis (TGA) profile and investigated. Fire retardancy-quenching mechanism is mapped out on the basis of input from solid state nuclear magnetic resonance spectroscopy (MAS NMR; ^{27}Al, ^{31}P and ^{13}C), Fourier transform Infra-red spectroscopy (FTIR), X-ray powder diffraction (XRD), electron probe microanalysis (EPMA), scanning electron microscopy (SEM), and optical microscopy on degraded samples. Gas phase analysis were studied by TGA coupled FTIR.

1. Introduction

Engineering polymers have become integral components of productions in E&E industries, transport industries, textiles and upholstery.[1-8] Their inherent flammability which often undermine their performance was successfully tackled by Flame retardants (FR) and related technologies.[1-8] Evolving tailor-made FRs particularly showcasing multi-functionality and end-of-life ecological concern,[9-11] revitalised and diversified the usage of engineering plastics. Contemporarily, elucidation of mechanism of action of FRs that interrupt the 'fire cycle' have been perceived as an indispensable investigation that provides crucial information on several aspects like, mode of action, compatibility-stability-performances of polymers, FR redesign strategy, fire safety engineering, theoretical modelling, and waste disposal.[12-25]

FRs that can maintain a fine equilibrium between efficiency parameters and environmental aspects like nitrogen based compounds are of high demand in FR market. Melamine based compounds belong to this category.[12-26] They provide greater efficiency, high decomposition temperature, moderate to low loading, synergism with phosphorus based FRs, less interference with stabilizers etc. On the other hand such FRs are also environmental friendly as they evolve less corrosive and toxic gases during combustion. This is due to the absence of by-products like dioxin and halogen acids. Such FRs are also found to have minimum issues with recyclability and landfilling.[9-11]

Recently[26] we investigated fire performance of Safire® in combination with aluminium phosphinate in glass fibre reinforced polyamide 66. Safire® series is based on melamine intercalated metal polyphosphates patented by Wehner and Dave.[24,25] Safire®200, (Melamine-poly(aluminum phosphate)) is one among them (Figure 1a). The supramolecular topology of Melamine,[27] variable coordinating ability of aluminium and dual action of binding/anion by phosphate makes metal integrated melamine polyphosphate family a unique combination of FRs which is expected to eventually influence the trajectory of flame retardancy.

Organic-inorganic hybrid molecules like Safire®200 can be perceived as higher analogue of melamine polyphosphate (MPP). Conceptually they can also be viewed as melamine directed or templated anionic aluminium phosphates of the type $AlPO_4$-n (n-denotes specific structure type). $AlPO_4$-n segment in such systems with an [Al]/[P] ratio of less than unity display rich diversity in structure and composition.[28-30] The diversity is due to the occurrence of coordination numbers greater than four

for aluminium atoms and the existence of terminal P-O bonds. This is in contrast to neutral $AlPO_4$-n framework with an [Al]/[P] ratio of exclusive unity, that are constructed from the alternation of tetrahedrally coordinated aluminium and phosphorus atom.[28] In fact a large variety of anionic aluminophosphates with zero-dimensional (0D) clusters, 1D chains, 2D layers, and 3D open-framework structures have been synthesised using organic amines (also using quaternary ammonium salts) as templates which plays structure-directing, space-filling or charge balancing molecules.[28-30] Mostly the non-bonding interaction between template and inorganic layers are dominated by H-bonding and van der Waals interactions.[28]

In anionic aluminophosphates, there are three types of aluminium coordination, AlO_4, AlO_5 and AlO_6 and depending upon its site distribution it can adopt diverse topologies. Further depending on the [O]/[P] ratio, the P-O-Al network may consists of a cross-linked network of Q^3 tetrahedra to polymer-like metaphosphate chains of Q^2 tetrahedra to 'invert' glasses based on small pyro- (Q^1) and orthophosphate (Q^0) anions. Such systems with 'tagged' nuclei (^{27}Al, ^{31}P) can be easily probed by solid state NMR techniques to map their structure-function relationship.[31,35] Safire®200 fits into this category.[27] Based on the molecular arrangement of melamine phosphate and related structures, it is assumed that melamine chains in Safire®200 are stacked in the crystal lattice and alternated by anionic chains of $AlPO_4$.[27]

There are several comprehensive reports on mechanistic aspects of melamine based flame retardants in polyamides.[12-23] Our investigation has been focused on elucidation of flame retardancy mechanism of Safire®200 and diethyl aluminium phosphinate (1:2 ratio, total 18wt.-% of flame retardants) blended glass fibre reinforced polyamide-66 formulation. It has been appropriately supported by investigation on decomposition of neat Safire®200, and single additive (Safire®200) blended glass fibre reinforced polyamide-66. Further supplementary data are recorded on neat polymer, diethyl aluminium phosphinate (Fig. 1b), and diethyl aluminium phosphinate blended polymer. The key evolving species in the decomposition pathway of these formulations which would have lethal effect on fire cycle were examined with solid state nuclear magnetic resonance spectroscopy (NMR), Fourier transform Infra-red spectroscopy, (FTIR), and X-ray powder diffraction (XRD). Samples at different stages of degradation were collected based on heat release rate (HRR) curve from cone calorimetry. Samples were also annealed in tubular furnace based on thermal degradation pattern obtained from thermogravimetry. The gaseous products released during combustion of these formulations/additives were identified by TGA coupled FTIR. Textures of intumescence/char were studied with optical microscope, electron probe microanalysis (EPMA), and scanning electron microscope (SEM). Based on the above results, the flame retardancy mechanism is elucidated.

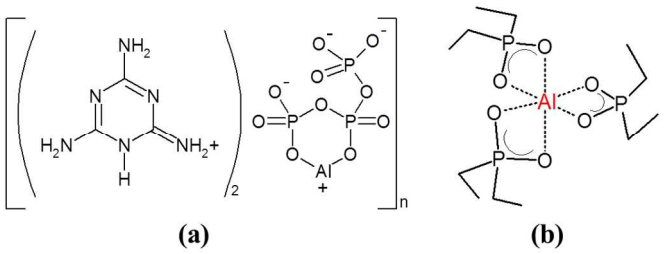

Fig. 1. (a) Molecular structure of Safire®200 (b) molecular structure of diethyl aluminium phosphinate, AlPi.

2. Experimental

2.1. Materials

Abbreviations for the materials used are given in bracket and are followed throughout this work. Polyamide 66 reinforced with 30 % glass fibers (PA66/GF) was supplied by Rhodia engineering plastics (St Fons, France), Melamine polyphosphate with trade name, Melapur200 (MPP) was from Ciba/BASF (Ludwigshafen, Germany), Diethyl aluminium phosphinate with trade name of Exolit OP1230 (AlPi) was from Clariant (Knapsack, Germany). Safire product, Safire®200 (Melamine-poly(aluminum phosphate), $\{(MelH)_2[Al(P_3O_{10})]\}_n$) was kindly provided by *Catena Additives a fully owned subsidiary of Floridienne Group (Ath, Belgium)*. Safire®200, is referred to as S200 hereafter.

2.2. Formulations, processing and sampling

2.2.1. Formulation and processing:

Compounding of formulations (Table 1) were performed using HAAKE Rheomix OS PTW 16 twin screw extruder as described in our previous paper.[26] All the materials were dried at 80 °C under vacuum for 24 hr prior to extrusion.

2.2.2. Sampling:

Samples for the study were collected from two sources (Table 1). One is from cone calorimetry experiment which is based on HRR curve[26] (Figure 2a) wherein sample (100 x 100 x 3 mm^3 plates) exposure to heat flux were stopped and withdrawn approximately at 100, 300, 600 and 1000s by closing the shutter between heating coil and the burning sample. Flaming can be extinguished manually by rapidly blanketing the test plate. A 4x4cm piece is scooped out from the central part of these plates including the intumescence part. The 600 and 1000s samples are manually crushed and collected. Samples at 100s and 300s are hard and are crushed into small pallets and ground in liquid nitrogen in an ultracentrifuge mill to produce a powder. Samples were dried at 80 °C under vacuum for 24 h and stored. These samples are used for all the analysis. The intended (100 to 1000s) time selection for sample collection is principally based on HRR profile of PA66/GF+AlPi+S200 formulation

which approximately denotes ascending, peak, descending and end of decomposition respectively. The same profile is extended for single additive formulations and neat PA66/GF. Most of the results investigated are based on these tests. Pyrolysis was performed in tubular furnace under nitrogen atmosphere. At the selected temperature, the sample placed in ceramic boat is introduced into the quartz tube fixed inside the tubular furnace and kept for 3 hr. The temperature selection is derived from TGA profile of formulations/additives which corresponds to temperature of maximum weight loss in each step performed at heating rate of 20°C/min under nitrogen atmosphere (Figure 2b). To have an insight into the mutual interactions between additives, additive mixture (AlPi+S200 in 2:1 ratio as in formulation) were also pyrolysed in tubular furnace and the decomposed samples were studied (Table 1). Decomposed samples studied in the present work were labelled with a name followed by a number. This number indicates either the time at which the cone experiment is stopped (approximately 100, 300, 600, or 1000s) or temperature of maximum degradation in each step of TGA curves (Table 2). Few samples were also annealed at 750°C in tubular furnace (Table 1). Results of tubular furnace experiments are supplementary and included only wherever necessary in the paper.

Table 1. Materials investigated in the present study and conditions of sample collection

Materials[1]	Sample collection time [2] (in second)	T (°C) profile[3]
PA66/GF+AlPi+ S200	100, 300, 600, 1000	323, 430, 581
PA66/GF+S200	100, 300, 600, 1000	382, 460
PA66/GF + AlPi	100, 300, 600, 1000	394, 462
PA66/GF (neat)	100, 300, 600	401
S200 (neat)	-	395,545, 750
AlPi (neat)	-	452, 510
AlPi+S200 (2:1 ratio, manually mixed)	-	323, 430, 581, 750

[1]AlPi: 12 wt.%; S200, 6 wt.%
[2]Based on HRR curve
[3]for tubular furnace experiment

2.3. Instrumental

2.3.1. Thermal analysis:

Thermogravimetric analyses (TGA) were performed using SDT Q600 (TA instruments). Samples (approx. 6-7 mg) were placed in open alumina pans covered with gold foil and heated under nitrogen atmosphere with a heating rate of 20°C/min.

2.3.2. Mass loss cone calorimeter:

The mass loss cone calorimeter (Fire Testing Technology (FTT)) is used for collecting sample for analysis. Plates (100 x 100 x 3 mm^3 plates) for cone calorimeter test were made via compression molding using DARRAGON press apparatus. Plates were wrapped in aluminium foil leaving the upper surface exposed to the heater and placed in horizontal position on ceramic block encased in a metallic container at a distance of 40 mm from cone base. External heat flux of 50kW/m^2 was used for all the experiments.

2.3.3. Spectral and XRD analysis:

FT-IR were recorded on Nicolet Impact 400 D in ATR mode at room temperature. X-ray diffraction (XRD) spectra were recorded using a Bruker AXS D8 diffractometer at RT. ^{31}P NMR measurements have been performed on a Bruker Avance II 400 at 40.5 MHz using a 3.2 mm probe, with/without cross polarization (CP, ^{1}H-^{31}P), with dipolar decoupling (DD) and magic angle spinning (MAS) at a spinning speed of 20 kHz. The delay time between two pulses was fixed at 120 s without CP. The reference used was 85% H_3PO_4 in aqueous solution. ^{27}Al NMR measurements have been performed on a Bruker Avance II 400 at 104 MHz using a 3.2 mm probe, with MAS at a spinning speed of 20 kHz. The delay time between two pulses was fixed at 1 s. The reference used is 1 M solution of aluminum nitrate. ^{13}C NMR measurements have been performed on a Bruker Avance II 400 at 100.4 MHz using 3.2 mm probes, with CP ^{1}H-^{13}C, dipolar decoupling (DD) and magic angle spinning (MAS) at a spinning speed of 10 kHz. For all samples, a delay time between two impulsions of 5 s and a contact time of 1 ms were used. TMS is used as reference for the chemical shift.

2.3.4. Microscopy:

Morphology of samples was studied using scanning electron microscope (SEM), Philips XL30 ESEM/EDAX-Sapphire with an accelerating voltage of 6 kV. VHX digital optical microscope (Keyence, VH-Z 100R) was used to investigate texture of samples. An electron probe microanalyser (EPMA) using wavelength dispersive X-ray spectrometers was used to perform elemental analysis. The char surface was transferred on a conductive carbon tape and carbon coated with a Bal-Tec SCD005 sputter coater. Elemental mapping (Si, P, Al, Ca) was performed over an area surrounding a glass fibre. The analyses were carried out at 15 kV 15nA for back scattered electrons (BSE) images and elemental analyses, and at 15 kV 40 nA for silicon (Si), Calcium (Ca), Phosphorus (P), and aluminum (Al) X-ray mappings. For mappings, a TAP crystal was used to detect the Si and Al Kα X-ray, and a PET crystal to detect the Ca and P Kα X-ray.

2.3.5. TGA-FTIR analysis:

Gas phase analysis were carried out in TGA Q5000 (TA instruments) coupled with FTIR Nicolet spectrometer (ThermoFischer). Samples (~5 to 15mg) were heated in a 100 µL alumina crucible from 50°C to 800°C with a heating rate of 10°C/min under nitrogen atmosphere. A balance purge flow of 15 mL/min and a sample purge flow of 100mL/min was maintained. A transfer line with an inner diameter of 1mm was used to connect TGA and infrared cell. The temperature of transfer line and gas cell was kept at 225°C. Prior to this,

samples were kept for 2h under nitrogen stream. IR spectra were collected in 400-4000cm^{-1} spectral range.

3. Results

3.1. General remarks:

Results of cone calorimetry and parameters for all the formulations were described in our previous paper.[26] The curves of heat release rate (HRR) for selected formulations were shown in Figure 2a. As seen from HRR curve neat PA66/GF burns with pHRR (peak of heat release rate) value of 352 kW/m^2 (total heat release, THR, 76 MJ/m^2) and totally decomposed leaving behind only white glass fiber mesh. Addition of single component FR, like AlPi or S200 alone reduces the pHRR by 55 and 58 % respectively (THR, 35 and 43 MJ/m^2). The two additives' formulation, PA66/GF+AlPi+S200, exhibits significant reduction (80%) in pHRR value (THR of 36 MJ/m^2) and exhibit intumescence phenomenon. In addition, time to ignition is delayed considerably.

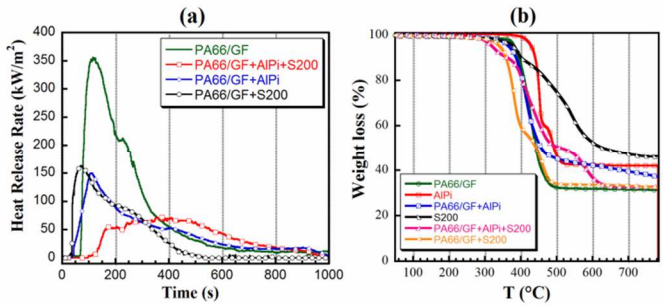

Fig. 2. (a) HRR curve from mass loss cone calorimetry[26] (b) TGA profile for additives and formulations.

Pyrolysis in tubular furnace represents different scenario compared to cone calorimetry in several aspects but the former provides useful information on additives. The thermal degradation in PA66/GF+AlPi+S200 (Fig. 2b, Table 1) is considerably changed compared to neat PA66/GF. Although initial thermal stability is less than that of neat PA66/GF, subsequent steps deviate significantly in terms of number of steps, abruptness, formation of stable intermediates, and weight loss. The major degradation step is more gradual than in PA66/GF and took place in two steps thus delaying the completion of degradation. Moreover there is a plateau between 490-540°C indicating the formation of stable species, possibly cross-linked material which degrades gradually stretching the degradation until 638°C unlike PA66/GF wherein the degradation is complete by 500°C.

Table 2. Thermal parameters derived from TGA profiles of additives and formulations (20°C/min, under nitrogen atmosphere).

Compound	Steps	T (°C) Range	Weight Loss (g)	Residue Weight (%)
PA66/30GF+AlPi+S200	3	278-353	9.42	32.9
		373-495	38.7	
		530-662	17.1	
PA66/GF+S200	2	313-408	42.1	32.1
		422-509	23.4	
PA66/GF+AlPi	1	341-504	53.1	35.7
S200	2	356-411	8.0	46.2
		430-773	43.8	
AlPi	2	420-466	40.2	42.3
		474-541	17.0	
PA66/GF	1	363-495	65.3	31.2

3.2. ^{27}Al and ^{31}P NMR characterisation on neat materials

3.2.1. S200 additive: In ^{27}Al MAS NMR of additive S200, signals appear in three distinct regions of spectrum (Table S1, Figure 3a). There must be three aluminium sites of $AlO_x(P)$ type with phosphorus bound oxygen. There is a strong peak at 39.2 ppm, slightly less intense signal at -17.7 ppm (in the ratio of 2:1) and a low intense signal at 12.1 ppm. Based on the reported data[19, 31-34] they are respectively assigned to AlO_4, AlO_6, and AlO_5 polyhedra which corresponds to aluminium with vertex oxygens connected to phosphorus. The ^{31}P CP MAS NMR shows three sets of peaks (Figure 4a). The peak position is indicative of PO_4 tetrahedra with varying degree of condensation/polymerisation. The low intense band at -10.3 ppm is assigned to pyrophosphate (Q^1) and/or terminal phosphate groups. Trace amount of orthophosphate is identified by a weak peak at 0 ppm. There are two sets of strong signals in the range of polyphosphate. The strong doublet at -21.2 and -24.3 ppm is assigned to middle groups of polyphosphate chain (Q^3, $P(=O)O_{3br}$; *br* is bridging) and is similar to that found in MPP. Peaks at -27.2 and -30.8 ppm are originating from $AlPO_4$ groups and this entity is more close to proton source from melamine molecule possibly connected by hydrogen bond. This is evident when NMR is run without HPDEC (high-power proton decoupling) experiment wherein the two peaks considerably decrease in intensity. Based on the molecular structure of MPP it can be presumed that melamine is intercalated between $AlPO_4$ layers. Further a significant change in crystal packing is also expected due to the presence of chelating aluminium.

3.2.2. PA66/GF+S200 formulation: Both ^{27}Al and ^{31}P NMR spectra look similar to that of S200 in terms of peak position but differ with respect to intensity of peaks. Thus the intensity of peak in ^{27}Al MAS NMR at -17.9 ppm is higher than that at 39 ppm (Fig. 3b). The broad resonance around 50 ppm is due to aluminium in silica network originating from glass fibre present in PA66.[16] Peaks in ^{31}P MAS NMR at -21.7 and -24.3 ppm are less intense than peaks at -27.3 and -31 ppm (Fig. 4b). These intensity differences are due to supramolecular interaction of S200 with the matrix.

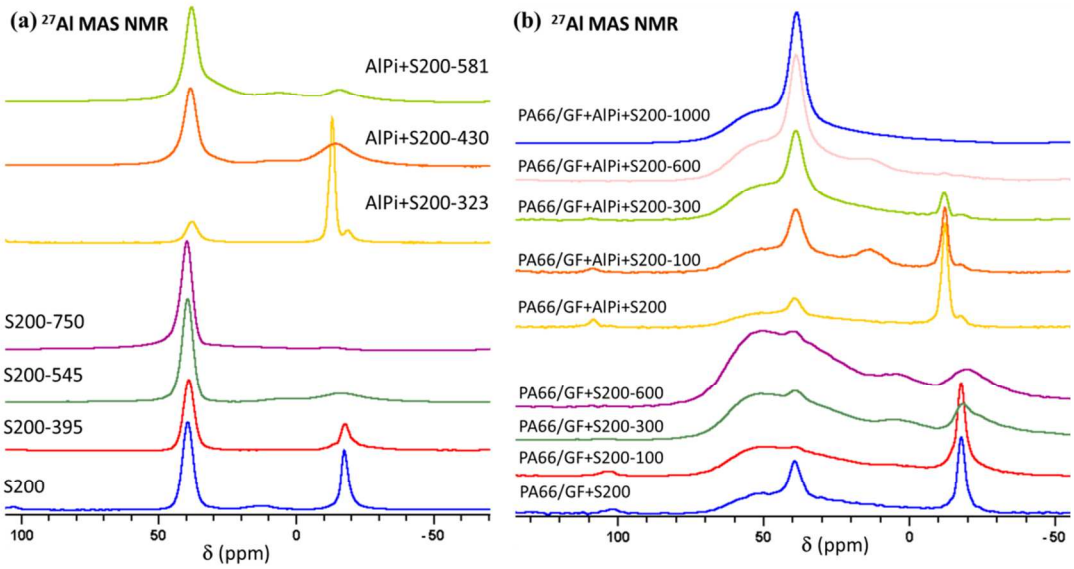

Fig. 3. ^{27}Al MAS NMR spectra on (a) S200 and its pyrolysis products at 395, 545, 750 °C and also for S200+AlPi mixture at 323, 430, 581 °C carried out in tubular furnace. (b) Degradation samples of formulations from cone calorimetry. 100, 300, 600, and 1000 are time (in second) at which the degrading polymer plates under the heat flux are dismounted.

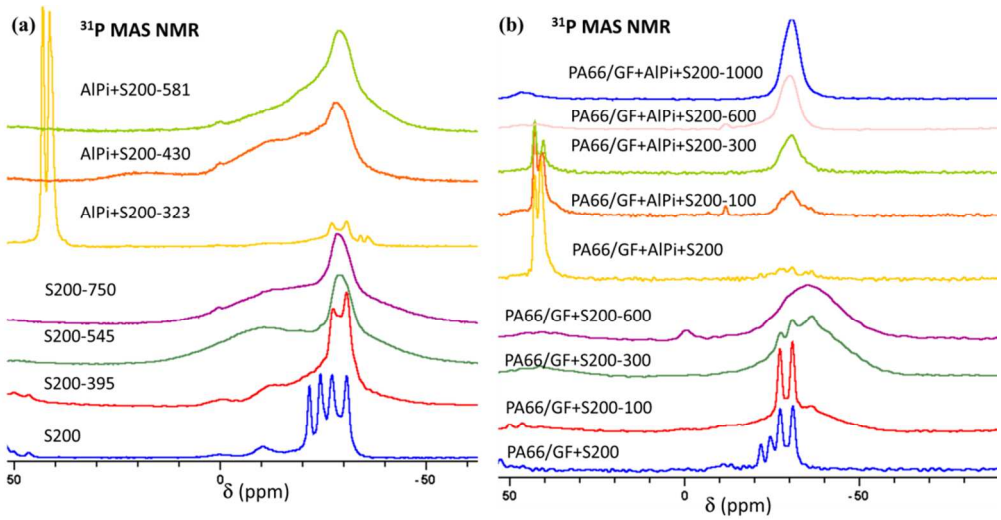

Fig. 4. ^{31}P MAS NMR spectra on (a) S200 and its pyrolysis products at 395, 545, 750 °C and also for S200+AlPi mixture at 323, 430, 581 °C carried out in tubular furnace. (b) Degradation samples of formulations from cone calorimetry. 100, 300, 600, and 1000 are time (in second) at which the degrading polymer plates under the heat flux are dismounted.

3.2.3. PA66/GF+AlPi+S200 formulation: ^{27}Al MAS NMR (Fig. 3b) shows four distinct signals. The broad signal around 54 ppm is due to alumina in glass fibre. Peaks corresponding to S200 are found at the same chemical shift as those of neat S200 (39.4, -17.5 ppm). Thus due to spectral similarity between neat S200 and PA66/GF+AlPi+S200, it is assumed that S200 having $AlPO_4$ network with melamine vicinity retains its identity in polyamide matrix. The strong signal at -12.2 ppm in ^{27}Al MAS NMR is assigned to aluminium in AlPi[16,19] that corresponds to octahedral AlO_6. ^{31}P CP NMR shows a doublet of equal intensity (42.9, 41.2 ppm) and this is likely to be due to two crystallographic sites or polymorphism in AlPi. Phosphorus signal of S200 is hardly visible.

3.3. NMR characterisation of degraded samples

All PA66/GF based materials show a broad signal around 51 ppm which was assigned to alumina in glass-fibre[16] and

appeared at the same chemical shift in all residues of formulations irrespective of level of decomposition. During the combustion process, polymer and organic part of additives begin to decompose and are released progressively and the well-ordered structure collapse. Stable inorganic units are left behind which restructure to form aluminophosphate frameworks (-Al-O-P-) composed of AlO_4 and PO_4 units. Although matrix/additives elimination brings closer inorganic units and induces a progressive polymerisation of aluminophosphate their restructuring into pure crystalline phase of $AlPO_4$ with definitive structure is seriously affected by several factors. Some of the factors are, the uncontrolled heating and subsequent cooling process, deviating [Al]/[O] ratio, formation of large amount of char, and formation of P-O-C bonds.

3.3.1. ^{27}Al MAS NMR probe for decomposition steps:

The AlO_6 and AlO_4 sites of $AlPO_4$ network of S200 and AlO_6(-P-C) in AlPi are the primary probing sites in PA66/GF+AlPi+S200 formulation to navigate through degradation pathway. As seen in the previous section, the three above mentioned sites are clearly distinguishable from one another in ^{27}Al MAS NMR by their characteristic chemical shift (S200: AlO_4(-PO) at 39.2 ppm; AlO_6(-PO) at -17.7 ppm and ^{31}P resonances at, 0, -10.3, -21.7, -24.4, -27.2, -30.8 ppm. AlPi: AlO_6(-P-C) at -12.2 ppm and its ^{31}P resonances, AlO_6(-PC) are at 42.9 and 41.2 ppm.

PA66/GF+AlPi+S200-100 sample (Fig. 3b) which represents the initial period of exposure to heat flux, display two changes. There is an increase in intensity of peak at 39.6 ppm and appearance of an additional small peak at 13.4 ppm. From 300 to 600s, there is further increase in intensity of the peak at 39.6 ppm at the expense of other two peaks at -12.2 and -17.7 ppm. The latter two peaks are not seen in 600s spectrum and the 1000s spectrum is dominated by a peak at 39 ppm. S200 alone, when subjected to heat treatment (from 395 to 750 °C) exhibits similar changes and a dominant signal appear around 39 ppm. Physically mixed AlPi+S200 mixture and PA66/GF+AlPi formulation (not shown) also follows the same trend. This consistent NMR pattern is also observed in PA66/GF+S200 but the evolution of peaks varies slightly and is discussed at the end of section 3.3.2. Thus aluminum sites irrespective of coordination number, chemical surroundings and fire scenario revert to same final product of $AlPO_4$ type in the final decomposed state. The peak at 39.3 ppm is attributed to the AlO_4 tetrahedra. The weak band at 13.4 ppm identified as AlO_5 and is possibly a transition phase in this conversion from AlO_6 to AlO_4. Thus at higher temperature there is a final convergence of signals to stable four coordinated highly integrated AlO_4(-PO) species possibly through an intermediate AlO_5(-P) state.[31] This suggests that from AlO_6(-PO) to AlO_4(-PO) transition there is total reshuffling of organised network. The chemical shift position does indicate that these species are $AlPO_4$ type rather than aluminates.[31]

3.3.2. ^{31}P CP MAS NMR probe for decomposition steps:

Since phosphate tetrahedra adopt diverse mode of coordination like monodentate, bidentate, and bridging, annealing/burning has severe effect on the overall framework integrity and topology. During this treatment, as AlO_6 of $AlPO_4$ polyhedra collapse (as evidenced by ^{27}Al NMR spectra) rearrangements around phosphorus site is expected and NMR signal should reveal phosphate site re-distributions. In PA66/GF+AlPi+S200 formulation (Fig. 4), the only dominating signal in ^{31}P MAS NMR is doublet at 43 ppm of AlPi as signal from S200 component is hardly visible. At 100s, there is a broad band at -30.5 ppm and a band of low intensity at -11.7 ppm. There is a change in peak intensity of AlPi doublet signal due to degradation of its aliphatic part and subsequent evolution of new species. At 300s, the intensity of peak at -30.1 ppm increases in intensity and at 600s, the signals around 43 ppm due to AlPi disappears and the spectrum is dominated by an intense band at -30.2 ppm.

Similarly ^{31}P CP NMR of PA66/GF+S200 (Fig. 4b), AlPi+S200 mixture (Fig. 4a) and neat S200 (Fig. 4a), show (Table S1) at the end of combustion process a dominant peak around -30 ppm. But their evolution varies in comparison with PA66/GF+AlPi+S200 formulation. Fragmentations are evidenced in S200 and AlPi+S200 mixture which are annealed in tubular furnace and they both display similar evolution of phosphate group. ^{31}P CP MAS of S200-390 shows 3 resonances. The low intense peak at 0 ppm indicates the formation of phosphoric acid, and broad band at -12.6 ppm is due to pyrophosphate fragments (Q^1). The first two signals (-20.9, -23.9 ppm) from polyphosphate chain (in neat S200) disappear and the other two signals (-26.6, -30.2 ppm) begin to merge in this spectrum. Spectra at 545 and 750°C show a broad resonance around -10 ppm. It is mainly due to pyrophosphate species and may include signals for orthophosphate. Additionally there is also strong broad band around -30 ppm. It is found that resonance position shifting towards negative value indicates more shielded ^{31}P surroundings which specify phosphate polymerisation. This is consistent with tetrahedral phosphorus (as PO_4) in the framework of $P(OAl)_4$.[31]

Decomposition pathway in PA66/GF+S200 deviates from others. Phosphorus signals are clearly identified in ^{31}P CP NMR of PA66/GF+S200 spectrum compared to PA66/GF+AlPi+S200 formulation. But contrary to neat S200, peaks at -21 and -24 ppm are less intense than peaks at -27 ppm and -31 ppm. In the preceding section, we have seen similar peak intensity difference between AlO_4 and AlO_6 species between them. These differences indicate that there is an interaction between S200 and polymer matrix.

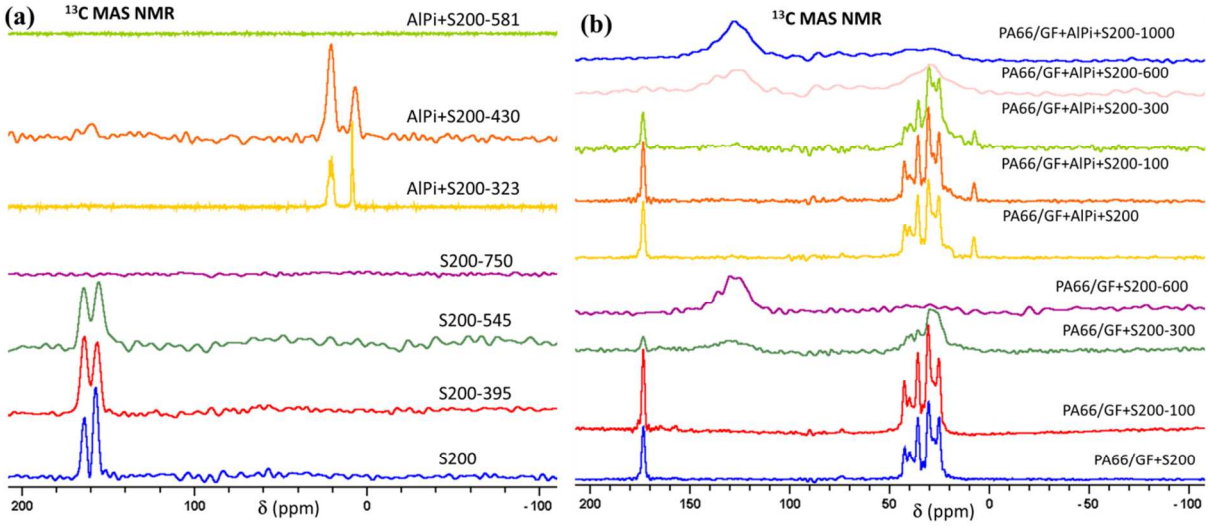

Fig. 5. ^{13}C MAS NMR spectra on (a) S200 and its pyrolysis products at 395, 545, 750 °C and also for S200+AlPi mixture at 323, 430, 581 °C carried out in tubular furnace. (b) Degradation samples of formulations from cone calorimetry. 100, 300, 600, and 1000 are time (in second) at which the degrading polymer plates under the heat flux are dismounted.

At 100s, the doublet (-21 and -24 ppm) in ^{31}P NMR spectrum of PA66/GF+S200, disappears (Fig. 4b). There is a broad signal between -20 to -40 ppm and a peak at -37 ppm. Peaks of $AlPO_4$ are still seen at -27 and -30 ppm. At 300s, peak at -37 ppm significantly increases in intensity. At 600s, there is a broad band between -17 to -50 ppm indicating the presence of multiple species.[36] Small amount of phosphoric acid is also detected at 0 ppm. The corresponding ^{27}Al MAS NMR (Fig 3b) also shows a broad bands between 40 to -20 ppm indicating the presence of multiple species. Thus it appears from NMR that PA66/GF+S200 follows different mechanism of decomposition.

3.4. ^{13}C MAS NMR characterisation of neat and decomposed materials:

Neat PA66/GF shows multiple peaks between 42.1 to 25.4 ppm and are assigned to aliphatic carbon chain. The carbonyl group appears at 173.3 ppm and is retained until 100s. No carbon compound is seen in 300s spectrum (Table S1). Neat AlPi shows a multiplet between 22.4-20.4 ppm and a strong peak at 8.6 ppm assigned respectively to $–CH_2$ and $–CH_3$ groups. Its insertion into PA66/GF increases the overall thermal stability of PA66/GF and signals corresponding to both PA66/GF and AlPi are found to be intact even at 300s. At 600s, carbon resonances are still visible between 8-20 ppm and a broad low intense resonance around at 130 ppm is seen which is assigned to char formation.[16,19,20]

In PA66/GF+AlPi+S200 formulation (Fig. 5b) only signals for PA66/GF and AlPi are observed and signal for S200 (164.4 and 157.5 ppm of triazine ring, described later in this section) could not be seen. Its 100s decomposed product is nearly similar. In the 600s spectrum, there is broad band around 128 ppm which is assigned to the formation of char. There is also an unresolved broad band around 29 ppm from degrading aliphatic segment of AlPi. Finally 1000s spectrum shows retention of only a strong broad band of char around 125 ppm. In PA66/GF+S200 formulation (Fig. 5b), only signal corresponding to PA66/GF is seen. The 300s spectrum still shows signals for aliphatic carbon (18-46 ppm) and carbonyl group (173 ppm) which indicate stabilization of PA66/GF network compared to neat PA66/GF. Char is also beginning to appear at this stage as evidenced by a broad signal around 129 ppm. Pyrolysis experiment also reveals similar results. At 460 °C, there is no polyamide 66 left behind, and two broad bands around 128 and 31 ppm are found and further at 600°C only dominating peak is that of char at 128 ppm. In general all composition leads to signal around 128 ppm due to char formation.

Neat S200 (Fig. 5a) has two bands at 164.4 and 157.5 ppm in the ratio of 1: 1.5 assigned to carbon atoms of triazine ring. Melamine in tautomeric forms or in salt form, can show two signals in ^{13}C NMR spectrum.[27] These signals have undergone changes in terms of intensity ratio upon annealing and this ratio is equalised at 395°C and also broadened. These observations indicate the presence of multiple species possibly due to de-ammonation leading to condensation products of melamine.

There are three main de-ammonation and condensation products of melamine – melam, melem and melon.[37,40,57,58,61,62] Tentatively, they are formed between 340-400°C, 400-450°C and 450-500 °C respectively with certain degree of flexibility in temperature range and shown to vary with experimental condition.[57,58,61,62] S200 may pass through one or more of these

phases during its pyrolysis. When S200 is heated to 395°C de-ammonation and self-condensation leads to formation of melem and could pass through melam intermediate.[57] The two resonances in NMR spectrum (Fig. 6) of S200-395 (163.9, 156.4 ppm) are very broad and along with melem it may include melam, and melamine-melam adduct. Since melam was found to have chelating ability as shown by several melam-metal complex,[40,62] it is reasonable to assume that aluminium vicinity could stabilise this intermediate. Conversion to any condensation product changes the electronic equivalence of carbon in the triazine ring ($CN_2(NH)_x$ and CN_3 moieties) and thus appearance of separate resonance. Since they are hardly separable, the signals are very broad. Further evidence about these species is given in FTIR section. ^{13}C NMR spectrum of S200-545 shows further broadening of ^{13}C NMR signals (163.8, 156.6 ppm) and there is noticeable shift of high-field side signal (156.6 ppm). At this stage condensation of melem sets in and oligomeric or polymeric heptazine based materials like melon or even small amount of its proton lacking counterpart graphitic carbon nitride (CN_x) would exists.

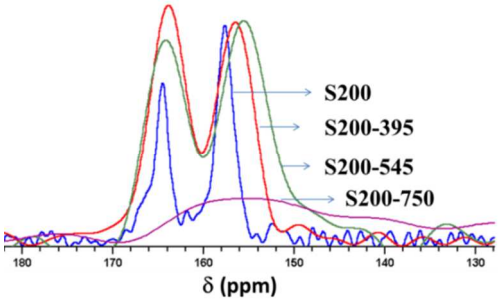

Fig. 6. Expanded region around aromatic carbon in ^{13}C CP MAS NMR of pyrolysed products of S200

In the ^{13}C NMR of S200-750 (after long acquisition), a low intense broad resonance around 156 ppm appears (Fig. 6). It is expected that as this is in the maximum degradation stage, the observed signal could be due to remaining incompletely decomposed melon and/or CN_x fragments.

3.5. FT-IR spectral results:

In case of neat S200, bands corresponding to $-NH_2$/NH stretch (Fig. 7) are seen between 3395-3157 cm^{-1}. The strong band at 1673 cm^{-1} is assigned to NH_2 bending. Signals arising from $AlPO_4$ group pertaining to -P-O and P-O-Al vibrations are also observed (Table S2).[16] Further the prominent band at 783 cm^{-1} is assigned to triazine ring bend.[38, 61, 62]

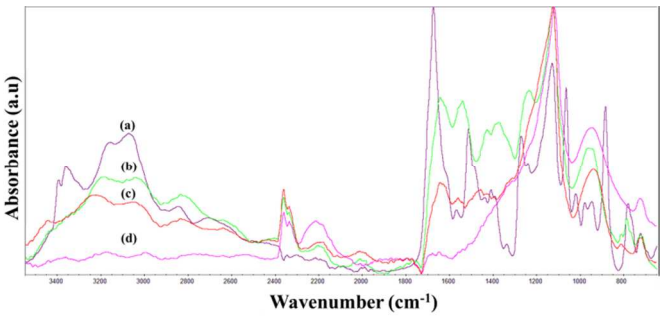

Fig. 7. FTIR of S200 and its degradation products. (a) S200 (b) S200-395 (c) S200-545 (d) S200-750

All the characteristic bands of organic part begin to decrease in intensity upon thermal treatment (395 °C to 545 °C to 750 °C). In 395°C spectrum, the $-NH_2$/-NH stretch around 3370 cm^{-1} and $-NH_2$ bend at 1673 cm^{-1} considerably decreases indicating involvement of amino group in condensation of melamine ring. Two new intense bands (1643, 1542 cm^{-1}) are found and are assigned to $\delta(NH_2)$ and ν(C=N) respectively of new species of melamine condensate. This has close similarity to IR spectrum of reported melem type structure.[37,61,62] In addition, new bands around 1370 and 1236 cm^{-1} are also seen and are due to characteristic C-NH-C unit of melam fragment indicating co-existing species. The S200-545 spectrum is similar to S200-395 spectrum but with reduced intensity of certain bands. There are also new bands thus the material may contain in addition to melem, oligomers of melem or melon type materials. Sample at 750°C is dominated by bands at 1118, 943, 726 and 464 cm^{-1}. These bands are normally very broad and may contain several vibrations related to P-O bond (P-O stretch, PO_2, Al-O-P and P=O stretch)[16, 38] and possibly P-O-C bands.[39] Interestingly, final degradation products from all the formulations (Fig. 8) display major bands in two regions 1050-1280 cm^{-1} and 820-1150 cm^{-1} indicates that the final residue obtained in all cases have similar composition and these results are consistent with solid state NMR. FTIR of PA66/GF+S200-1000 is slightly different and the difference in evolution of species is also evidenced in NMR. It should be noted that glass fibre in the residue of formulation also give strong signal in FTIR around 940 and 712 cm^{-1}.

The strong bands in the spectra of S200-395 and S200-545 indicate that the degradation in S200 proceeds through gradual de-ammonation and condensation process in addition to sublimation. Another noticeable feature in 750°C spectrum is a broad distinct band around 2210 cm^{-1} possibly due to formation of a nitrile or cyanamide derivative which is also seen in pyrolysed product of MPP under similar condition.[38] It has been observed that if melamine is heated above 650°C it is partially cracked due to de-polymerisation, leading to cyanamide along with other products especially in the absence of oxygen.[37] It is also reported that at elevated temperature, heptazine may partly

be broken-off giving dicyandiamide, cyanamide and ammonia.[62]

As the S200 degradation materials are collected based on temperature of maximum degradation in TGA curve it is likely that the samples are mixture of products rather than single phase of any melamine condensate. Also thermal treatment time duration (3h) may not be sufficient for complete transformation into a single species. This is apparent from aforementioned discussion of FTIR and NMR. For the same reason distinct identification of melon and carbon nitrides is dubious. It has to be noted that polymeric condensate melon is often highly colored (yellow or brown) due to conjugation. The color change in S200 is not so intense, off-white at 545°C to cream at 750°C.

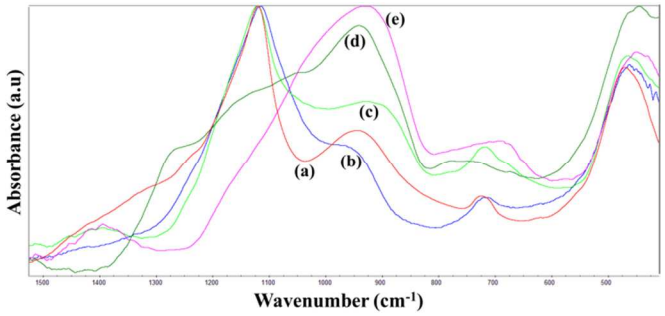

Fig. 8. FT-IR on residue of selected compounds (a) S200-750 (b) AlPi+S200-750 (c) PA66/GF+AlPi+S200-1000 (d) PA66/GF+S200-1000 (e) Glass fibre

3.6. X-ray powder diffraction studies (XRD):

XRD peaks of S200 are sharp and indicate its crystalline nature (Fig. 9Aa). At 395 °C, the XRD pattern indicates network collapse as some of the peaks disappear and some are broadened. From 545 °C onwards major diffraction peaks are restricted between 20-22° (Table S2) and a weak peak is seen around 35°. Except slight change in peak position/intensity all final residues collected above 700°C shows similar patterns. At higher temperature (Figure 9f, g) the broad band seen between 20° and 30° is attributed to char formation. This residue could be mixture of different $AlPO_4$ [43-47] with varying composition and small amount of alumina cannot be excluded. In fact due to cascade of several phase transitions at elevated temperatures $AlPO_4$ could crystallises in several modifications like hexagonal, triclinic and monoclinic tridymites, cristobalite, or Berlinite.[43-47] Some of the main distinct XRD peaks at 20.7, 21.8, and 35.5 (°) which are present in all residues have close resemblance to the XRD pattern of some of the known $AlPO_4$ forms like tridymites.[43] XRD search and fitting procedure[48] helps us to identify the species that partly fits with monoclinic and triclinic (pseudo-orthorhombic) $AlPO_4$ tridymites type (Fig. 9B). These results also support our earlier observation of similarity among residues from different sources. Again, as in NMR and FTIR data, the XRD peak intensity ratio is slightly different in PA66/GF+S200-1000.

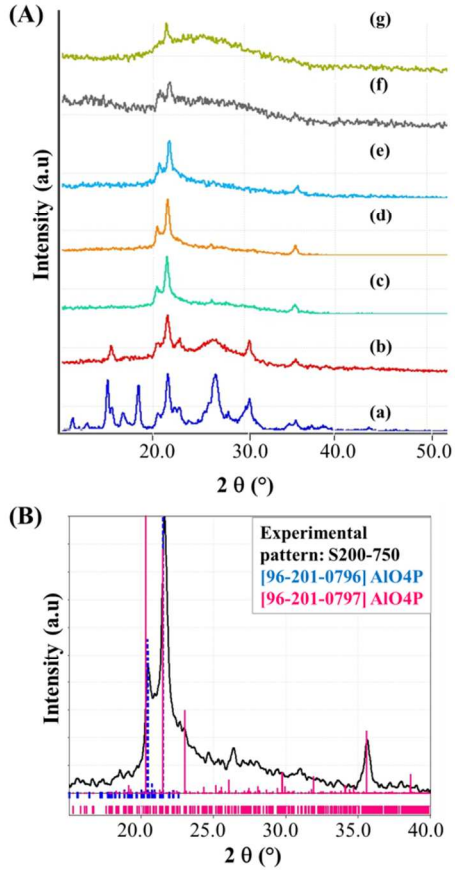

Fig. 9. (A) XRD pattern for selected compounds (a) S200 (b) S200-395 (c) S200-545 (d) S200-750 (e) AlPi+S200-750 (f) PA66/GF+AlPi+S200-1000 (g) PA66/GF+S200-1000 (B) Comparison of experimental XRD data on S200-750 to reference pattern.

3.7. Texture studies on degradation products

PA66/GF+AlPi+S200 formulation shows significant intumescence under heat flux during cone calorimetry experiment (Figure 10a).[26] It is hollow and crack free during its formation. Optical image on intumescence surface shows highly shiny/glazed surface (Figure 10b). This surface is finely supported by glass fibres which is evident when this surface is viewed on its underside (Fig. 10c). Under the heat flux the bulging intumescence which regulates the mounting pressure from inside develops numerous 'cell' like protrusions. There are also some concavities distributed on the surface which probably leads to microscopic pores. A 3D image around such area is shown in Figure 10d. Intumescence still holding/resisting the heat flux and stretching the degradation along, the underneath material burns in such a way that highly porous carbonaceous structure/char is formed resembling sponge type material. The channels in the porous structure are (Fig. 10e) interconnected and a 3D view on sponge like char showing interconnectivity is shown in Figure 10f. The building-up of this structure during burning condition is due to extreme

cross-linking. This may act as an additional thermal insulation to the underlying unburnt materials by physical shielding.

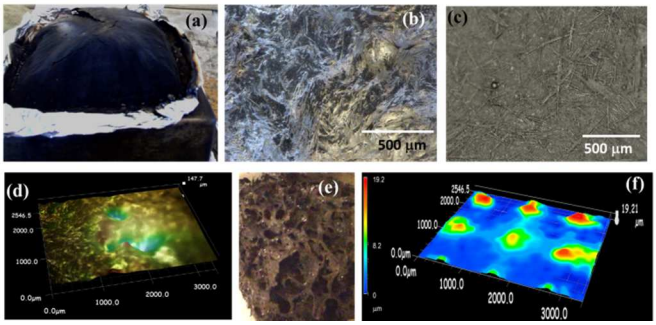

Fig. 10. Images on PA66/GF+AlPi+S200 formulation after cone calorimetry test (a) View of Intumescence (b) Optical microscope image on the surface of intumescence (c) Optical microscope image on lower side of the intumescence (d) 3D topography on the intumescence surface around concavities (e) Cross-section view on the base portion of the residue showing porosity. (f) 3D view on previous image showing interconnected porosity.

AlPi (powder) alone in tubular furnace shows interesting physical response.[19] Around 450 °C, part of the AlPi sublimates and recrystallizes on the wall of the quart tube (Fig. 11a) as needle shaped colorless crystals. Its identity is confirmed by FTIR. At higher temperature (550 °C) AlPi decomposes and results in swelled porous structure (Fig. 11b) which has highly shiny reflective surface (Fig. 11d) but the corresponding surface in PA66/GF+AlPi in cone experiment is highly amorphous.

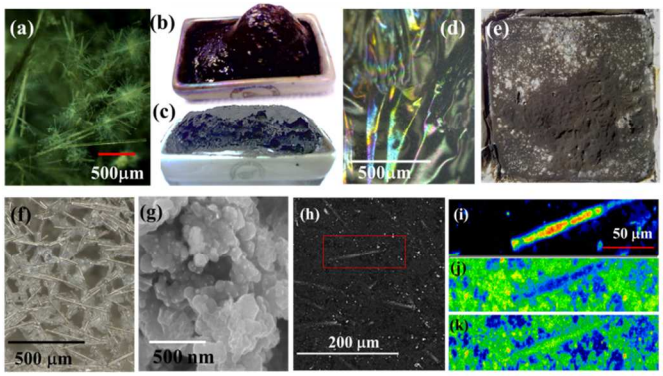

Fig. 11. (a) re-crystallized AlPi during thermal treatment in tubular furnace (b) Response to controlled temperature increment in tubular furnace on AlPi (c) Cross-section showing porous layers in PA66/GF+S200-750 (d) Glazy surface of AlPi residue (e) Residue obtained after cone calorimetry test in PA66/GF+S200-1000 (10x10x0.3 cm^3 plate) (f) magnified image on its surface (g) SEM image on PA66/GF+AlPi+S200-750 (h) BSE image on carbon coated intumescence surface of PA66/GF+AlPi+S200. White needles are glass fibres and bright spots are agglomerates rich in Al-P. (i) Silicon mapping in glass-fibre (j) Surface is rich in phosphorus except in the areas of glass-fibre (k) Distribution of aluminium including the area of glass fibre.

Intumescence phenomenon is less significant in case of PA66/GF+S200 formulation (Fig. 11e), and the morphology studies shows a highly porous surface loosely supported by glass fibres (Fig. 11f). The same formulation (2x1x0.3 cm^3 plate) in tubular furnace acts in different way. The swelled structure under cross-section shows layers of char (Fig. 11c) unlike hollow intumescence. The glazy intumescence surface in PA66/GF+AlPi+S200 is also studied by EPMA to map the distribution of elements. The BSE images and elemental mapping are performed around a glass-fibre including white agglomerates (Fig. 11h), and are shown in Fig. 11i-k. It is found that the glazy surface is densely coated with $AlPO_4$ during intumescence development and is assumed to contribute to the formation of robust intumescence surface. No crystals or particles of definite texture corresponding to $AlPO_4$ are found among large quantity of char in SEM image (Fig. 11g), although small lumps of white particles are often found visibly in lower char layer.

3.8. TGA-FTIR studies:

The evolved gas analysis carried out for PA66/GF+AlPi+S200 is displayed in Figure 12 and compared with PA66/GF+S200, PA66/GF+AlPi and PA66/GF as 2D counter map in Figure 13. Identification of gases in the FTIR spectrum is based on earlier reports and pertaining to characteristic bands.[16,19, 49-51] Aliphatic fragments (3000-2800 cm^{-1}), CO_2 (2368, 667 cm^{-1}), NH_3 (963, 933 cm^{-1}), cyclopentanone (1767 cm^{-1}), nitrile derivatives (2229 cm^{-1}), water (4000-3500 cm^{-1}), carbon monoxide (2185, 2105 cm^{-1}), amine/amide fragments (3332, 1626 cm^{-1}) are most common volatiles observed in this gas phase analysis.

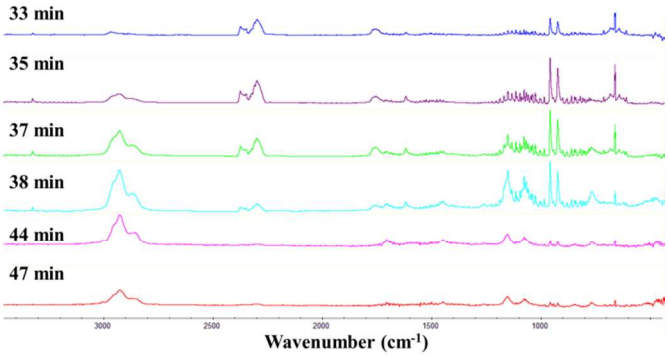

Fig. 12. TGA-FTIR of PA66/GF+AlPi+S200 formulation under N_2 atmosphere at selected time.

Neat PA66/GF shows no significant evolution of volatiles until 30 min (~300 °C). Thereafter simultaneous but gradual evolution of hydrocarbon, CO_2, cyclopentanone, and ammonia is started indicating cyclization route of depolymerisation. At 35 min (~350 °C) the evolution of cyclopentanone increases drastically along with other above mentioned gases. Around 40 min (~403 °C) cyclopentanone starts to decrease and hydrocarbon starts to increase along with ammonia. After 43 min (~436°C) there is only hydrocarbon evolution.

PA66/GF+AlPi+S200 follows completely different degradation pathway. Rather early, from 20min. (~229°C) very gradual evolution of CO_2 begins. At 27min. (~300°C), in addition ammonia starts to evolve. Around 30min. (~333°C) hydrocarbon and cyclopentanone evolution which has been negligible up to now starts to appear gradually along with CO_2 and NH_3 and continued up to 33 min. Small amount of amide is also seen in this period. This is inflection point of major degradation step in TGA. Around 36 min (~400°C) hydrocarbons begin to dominate. Soon after (37min.), AlPi (P-O, P=O stretch of AlPi; 1159, 1085 cm^{-1}) is seen[16] along with fractions of all other gases. At 40 min (~431°C) it is mainly evolution of hydrocarbon, along with small amount of AlPi and ammonia. AlPi is also clearly identified in the gas phase analysis of PA66/GF+AlPi formulation. There are no characteristic bands of melamine (1596 cm^{-1}) observed throughout the analysis. It is mainly due to chemical transformation of melamine component of S200 by de-ammonation and condensation. There is also possibility of recrystallization of melamine in the transfer line in case of partial sublimation. In fact, the only noticeable species evolved in the pyrolysis of neat S200 is ammonia.

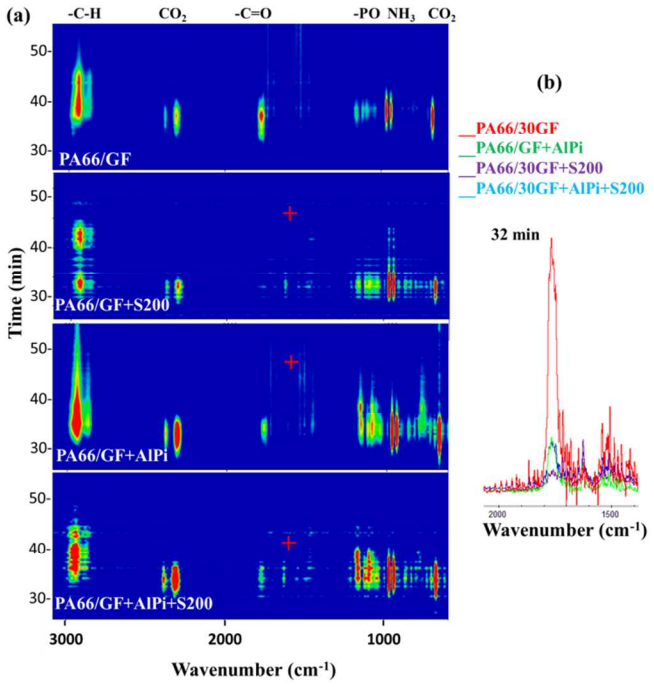

Fig. 13. (a) 2D counter map comparing evolution of species in different formulations. The bright red color indicates intensity of signals of particular evolved species. Selected functional group regions are indicated on the top (b) TGA-FTIR showing evolution of cyclopentanone in different formulations at 32 min.

In PA66/GF+S200, evolution of volatiles takes place in two instalments. From 28 to 37 min, there is simultaneous evolution of NH_3, CO_2, hydrocarbon and small amount of cyclopentanone. There is sudden drop in the evolution of gases around 38 min. possibly due to cross-linking and is evidenced in TGA profile wherein there is short plateau around this stage. In the second phase, after 37 min. (~390°C) mainly hydrocarbons and NH_3 are produced. At later stage (after 55 min.) mainly CO_2 and CO with small amount of hydrocarbon are produced. Figure 13b depicts the comparison of evolution of cyclopentanone in different formulations. Clearly, there is substantial amount of combustible cyclopentanone which is produced in case of PA66/GF compared to flame retarded formulations.

4. Discussion:

Unless flame retarded, PA66 without substantial cross-linking decompose completely.[52-56] Degradation of neat PA66 normally proceeds through depolymerisation that may involve cyclization of adipic acid portion of the chain (Scheme 1a) or polymer chain scission. The adipic acid component of the polymer is thought to be related to the cross-linking propensity of polyamide 66.[52] Cyclization of adipic acid portion produce cyclopentanone, a volatile product. This could happen either at adipic acid portion or chain ends of polymers. Both AlPi and S200 independently and also together are found to influence this degradation pathway.

During pyrolysis of formulations, it is found that release (Fig. 13b) of flammable cyclopentanone decreases significantly. This would mean that the major degradation pathway for PA66 is chain scission (Scheme 1b) that may provide polyamide fragments which are suitable for cross-linking. On the other hand it is also possible that released cyclopentanone reacts with additives or its by-products in the condensed phase and subsequently utilized in cross-linking process. As [O]/[P] ratio is changed during combustion, orthophosphoric acid, pyrophosphates, polyphosphoric acid and higher oxides of phosphorus with or without aluminium binding are formed and most of them are identified from solid state NMR. $AlPO_4$ is distinctly identified in the char and its evolution is traced from NMR: (AlO_6(-PO) to AlO_5(-PO) to AlO_4(-PO)). Such phosphorus based species are well-known key elements in the formation of insulating char by engaging in cross-linking mechanism. It is found from solid state NMR (Fig. 4) and XRD (Fig. 9) that both S200 and AlPi have mutual influences on their respective degradation pathway. S200 alone in PA66/GF fails to produce well-structured $AlPO_4$ but does so in the presence of AlPi. Moreover the possible matrix interaction of S200 (Fig. 3b) that change the course of PA66 decomposition (Fig. 13a) is minimised in the presence of AlPi (Fig. 3b). AlPi alone in PA66/GF at 600s (Table S1) still shows the degrading component of AlPi but no traces of it is seen in the presence of S200 (Fig. 4b) in PA66/GF+AlPi+S200-600. Since both S200 and AlPi have high probability of sublimation, they contribute to the swelling of intumescence (Fig. 10a). It has to be noted that neither S200 nor AlPi alone could produce such a significant intumescence (Fig. 11e).

Further de-ammonation products in the condensation cascade of melamine are regarded as flame retarding materials.[59,60] In the deammonation-condensation-degradation of S200, formation of melam, melem, oligomers of melem or melon/carbon nitride, cyanamide/nitrile derivatives are observed some of which might be stabilised with aluminium coordination. All these species provide substantial amount of raw materials for extensive cross-linking and formation of char/intumescence.

S200 like MPP may also decompose endothermically acting as a heat sink and reduce pHRR. TGA-FTIR gives strong evidence of release of ammonia that dilute oxygen and the flammable gases in the flame.[12-23] Cyanamide/nitrile type derivative identified in degradation of neat S200, like, melamine are also considered as blowing agent.[42] AlPi either alone or in dissociated form, or even phosphorus based radical form could act in gas phase of flame retardancy.

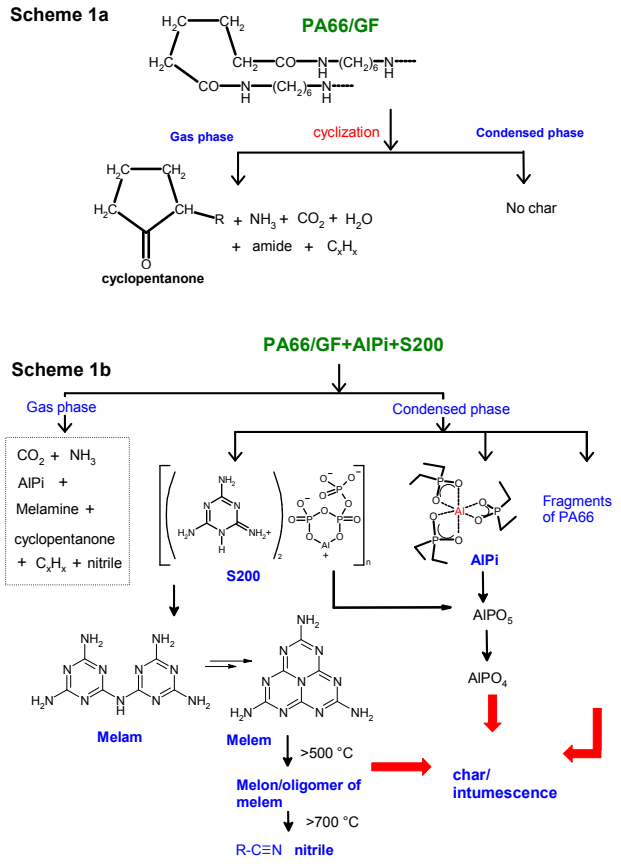

Scheme 1. Tentative degradation pathway in (a) PA66/GF (b) PA66/GF+AlPi+S200 and some of the key reactive species operating in gas and condensed phase mechanism.

In addition to this, the role of glass fibers is crucial in all these formulations. They not only retard melt flow and act as a 'wick' but also interwoven and reinforce the char/intumescence cohesiveness. Although major fire retardancy steps involving gas and condensed phase are similar to that observed in PA66/GF+AlPi+MPP formulation, additional feature like significant and robust intumescence are attributed to melamine integrated poly aluminium phosphate additive.

The experimental evidences discussed thus far signify that both S200 and AlPi contribute to the gas and condensed phase mechanism of flame retardancy. The global performance of PA66/GF+AlPi+S200 towards flame retardancy is credited to the synergistic effect of both additives. This includes intumescent behaviour, delay in ignition, reduction in pHRR, prolonging decomposition, and formation of key chemical species. Neither S200 nor AlPi alone could able to achieve these assets in their respective formulations.

5. Conclusion:

Foregoing discussion revolved around flame retardancy mechanism of a non-halogenated, environmental friendly FR, Safire®200 together with phosphorus compound diethyl aluminium phosphinate. This synergy has been efficient in deviating the usual degradation pathway of polyamide 66 and thereby giving substantial reinforcement in flame retardancy. Safire®200 or its contemporaries have molecular arrangement that can be further tailored based on the retrospective degradation pathway that has been fully elucidated. Their structure-performance can be tuned by incorporating MPO_x (M=metal ion) as secondary building blocks (SBU) under the concepts of crystal engineering to design functional coordination polymers and metal-organic frameworks in the realm of flame retardancy wherein essential elements needed for flame retardancy can be inserted in the post-synthetic stage.

6. Notes and references

[a]ISP/UMET – UMR/CNRS 8207, Ecole Nationale Supérieure de Chimie de Lille (ENSCL), Avenue Dimitri Mendeleïev – Bât. C7a, BP 90108, 59652 Villeneuve d'Ascq Cedex, France.

[b]Floridienne Chimie, 12 Quai des Usines, 7800 Ath, Belgium, *Corresponding author; e-mail: serge.bourbigot@ensc-lille.fr

† Electronic Supplementary Information (ESI) available: Solid state NMR data for additive, formulations and their degradation products are given in Table S1. X-ray powder diffraction data and FTIR spectral data on selected compounds are given in Table S2.

1. S. Bourbigot, M. Le Bras, and J. Troitzsch, Fundamentals: introduction, in: J. Troitzsch, (Eds), Flammability handbook, Munich, Hanser Verlag, 2003, 3-7.
2. B. Schartel, *Materials*, 2010, **3**, 4710.
3. S. Bourbigot, and S. Duquesne, *J. Mat. Chem*., 2007, **17**, 2283.
4. T.R. Hull, and B. Kandola, (Eds), Fire retardancy of polymers: New strategies and mechanisms. RSC Publishing, ISBN: 978-0-85404-149-7, 2008.

5. C.A. Wilkie, and A.B. Morgan, Fire Retardancy of Polymeric Materials, Second Edition, CRC Press, ISBN: 978-1-4200-8399-6, 2009.
6. A.R. Horrocks, B.K. Kandola and P.J. Davies, S. Zhang, S.A. Padbury, *Polym. Degrad. Stab*., 2005, **88**, 3.
7. E.D. Weil, Synergists, Adjuvants, and Antagonists in Flame-Retardant Systems. In Fire Retardancy of Polymeric Materials; A.F. Grand, C.A. Wilkie, (Eds), Marcel Dekker: New York, NY, USA, 2000; chap. 4:115-145.
8. http://www.pinfa.org/applications.html
9. van der Veen Ike and de Boer Jacob, *Chemosphere*, 2012, **88**, 1119.
10. Cynthia A de Wit, *Chemosphere*, 2002, **46**, 583.
11. H. Horacek, and R. Grabner, *Polym. Degrad. Stab*., 1996, **54**, 205.
12. S.V. Levchik, A.I. Balabanovich, G.F. Levchik, and L. Costa. *Fire and Mater*., 1997, **21**, 75.
13. A. Casu, G. Camino, M. De Giorgi, D. Flath , V. Morone, and R. Zenoni, *Polym. Degrad. Stab*., 1997, **58**, 297.
14. Y. Liu, and Q. Wang, *Polym. Degrad. Stab*., 2006, **91**, 3103.
15. S. Jahromi, W. Gabriëlse, Ad Braam, *Polymer*, 2003, **44**, 25.
16. U. Braun, B. Schartel, M.A. Fichera, and C. Jäger, *Polym. Degrad. Stab*., 2007, **9**, 1528.
17. L. Li, B. Li, and Feitang. *J. Reinforced plastics and composites*, 2008, **27**, 277.
18. L. Costa, G. Camino, M.P. Luda di Cortemiglia, Fire and Polymers, ACS Symposium Series, 1990, Chapter 15, **425**, 211-238, DOI: 10.1021/bk-1990-0425.ch015.
19. F. Samyn, and S. Bourbigot, *Poly. Degrad. Stab*., 2012, **97**, 2217.
20. M. Jimenez, S. Duquesne and S. Bourbigot, *Polym. Degrad. Stab*., 2013, **98**, 1378.
21. H. Seefeldt, E. Duemichen, and U. Braun, *Polym. International*, 2013, **62**, 1608.
22. P. Gijsmana, R. Steenbakkersa, C. Fürstb, and J. Kersjesc, *Polym. Degrad. Stab*., 2002, **78**, 219.
23. P.R. Hornsby, J. Wang, R. Rothon, G. Jackson, G. Wilkinson, K. and Cossick, *Polym. Degrad. Stab*., 1996, **51**, 235.
24. W. Wehner, and T. Dave, German Patent, DE 10 2007 036 465 A1, 2009.
25. H-G. Köstler, T. Dave, and W. Wehner, German Patent, DE 10 2010 035 103 A1, 2012.
26. A. D. Naik, G. Fontaine, F. Samyn, X. Delva, Y. Bourgeois, and S. Bourbigot, *Polym. Degrad. Stab*., 2013, **98**, 2653.
27. V. Brodski, R. Peschar, H. Schenk, A. Brinkmann, E. R. H. van Eck, A. P. M. Kentgens, B. Coussens, and Ad Braam, *J. Phys. Chem*., *B*, 2004, **108**, 15069.
28. J. Yu, and X. Ruren, *Chem. Soc. Rev.*, 2006, **35**, 593.
29. R. W. Dorner, M. Deifallah, D. S. Coombes, C. R. A. Catlow, and Furio Corà, *Chem. Mater.*, 2007, **19**, 2261.
30. M. Wang, J.Y. Li, J.H. Yu, Q.H. Pan, X.W. Song, and R.R. Xu, *Inorg. Chem*., 2005, **44**, 4604.
31. R. J. Kirkpatrick, and R. K. Brow, *Solid state Nucl. Magn. Reso.*, 1995, **5**, 9.
32. J.Quartararo, M.Guelton, M.Rigole, J-P. Amoureux, C.Fernandez, and J. Grimbolt, *J. Mat. Chem*., 1999, **9**, 2637.
33. G.Tricot, D. Coillot D, E.Creton, and L.Montagne, *J. Eur. Ceramic Soc*., 2008, **28**, 1135.
34. S. Duquesne, G. Fontaine, O. Cérin-Delaval, B. Gardelle, G. Tricot, and S. Bourbigot. *Thermochimica Acta*, 2013, **551**, 175.
35. R. Xu, W. Zhang, J. Xu, Z. Tian, F. Deng, X. Han, and X. Bao, *J.Phys.Chem.C* 2013, **117**, 5848.
36. M. Bugajny, S. Bourbigot, M. Le Bras, and R. Delobel, *Polym Int*, 1999, **48**, 264.
37. B. Jürgens, E. Irran, J.Senker, P. Kroll, H. Müller, and W. Schnick, *J. Am. Chem. Soc*., 2003, **125**, 10288.
38. L.Costa, and G.Camino, *J. Therm Anal*, 1988, **34**, 423,
39. S. Duquesne, M. Le Bras, S. Bourbigot, R. Delobel, G. Camino, B. Eling, C. Lindsay, T. Roels, and H.Vezin, *J. Appl Polym. Sci.*, 2001, **82**, 3262.
40. B. V. Lotsch, and W. Schnick, *Chem. Eur. J.*, 2007, **17**, 4956.
41. G.M. Crews, W. Ripperger, D.B. Kersebohm, T. Güthner, and B. Mertschenk, Ullmann's Encyclopedia of Industrial Chemistry, 2006.
42. B. Bann, and S.A. Miller, *Chem. Rev*., 1958, **58**, 131.
43. Y. Muraoka, and K. Kihara, *Phys. and Chem. of Minerals,* 1997, **24**, 243.
44. H. Graetsch, *Acta Cryst.,* 2000, **C56**, 401.
45. D. Zhou, L. Chen, J. Yu, Y. Li, W. Yan, F. Deng, and R. Xu, *Inorg. Chem*., 2005, **44**, 4391.
46. H. A. Graetsch, *Acta Cryst*. 2001. **C57**, 665.
47. H.A. Graetsch, *Acta Cryst.* 2002, **C5**8, i18.
48. Match, Phase Identification from Powder Diffraction, http://www.crystalimpact.com/match/.
49. S.Molyneux, A.A.Stec, and T. R.Hull, *Poly. Degrad. Stab*., 2013, http://dx.doi.org/10.1016/j.polymdegradstab.2013.09.013.
50. L. Liping, L. Bin, and F. Tang, *Europ. Polym. J*., 2007, **43**, 2604.
51. U. Braun, and B. Schartel, *J. Fire sciences*, 2005, **23**, 5.
52. M.A.Schaffer, E.K.Marchildon, K.B.Mcauley, and M.F.Cunningham, *J.Macromol. Science, C: Poly. Rev*., 2000, **40**, 233.
53. S.V. Levchik, and E.D. Weil, *Polym. Int.,* 2000, **49**, 1033.
54. S.V. Levchik, E.D.Weil, and M. Lewin, *Polym. Int.,* 1997, **48**, 532, 1997.
55. P. Gijsman, D. Tummers, and K. Janssen, *Polym. Degrad. Stab*, 1995, **49**, 121.
56. J. Bozi, Z. Czegeny, and M. Blazso, *Thermochimica Acta,* 2008, **472**, 84.
57. A. Sattler, S. Pagano, M. Zeuner, A.Aurawski, D. Gunzelmann, J. Senker, Klaus M-Buschbaum, and W.Schnick, *Chem. Eur. J.*, 2009, **15**, 13161.
58. A. Schwarzer, T. Saplinova, and E. Kroke, *Coord. Chem. Rev*., 2013, **257,** 2032.
59. T. Toshiyuki, and S. Ryo, Jpn. Kokai Tokkyo Koho, 2004, JP 2004010694 A 20040115.
60. S. Elke, N. Bernd, and W. Wolfgang, Eur. Pat. Appl. 2004, EP 1386942A1, 20040204.
61. E. Wirnhier, M.B.Mesch, J. Senker, W. Schnick, E. Wirnhier, M.B.Mesch, J. Senker, and W. Schnick, *Chem Eur J*, 2013, **19**, 2041.
62. B. V. Lotsch, PhD thesis, Ludwig Maximilians-Universitat Munchen, 2006